ELSEVIER

Physica D 121 (1998) 163–174

PHYSICA D

# A model of mixing and transport in wavy Taylor–Couette flow

Matthias Rudolph [a,1], Troy Shinbrot [b,2], Richard M. Lueptow [a,*]

[a] *Department of Mechanical Engineering, Northwestern University, Evanston, IL 60208-3111, USA*
[b] *Department of Chemical Engineering, Northwestern University, Evanston, IL, USA*

Received 23 September 1997; received in revised form 30 March 1998; accepted 31 March 1998
Communicated by J.D. Meiss

**Abstract**

Wavy Taylor vortex flow was simulated by developing a stream function model of the velocity vector field in a radial–axial plane that mimics an experimentally obtained velocity field. The simulation neglects the azimuthal component of velocity but provides estimates of the mixing and axial transport properties of wavy vortex flow in the axial–radial plane at higher Taylor numbers ($Ta$) and larger gap widths than previous models. Based on the estimated Lyapunov numbers, the particle paths appear to be chaotic for wavy vortex flow in the range $131 \leq Ta \leq 253$. The axial particle transport increases with the Taylor number in this range, most likely due to increased axial transport of fluid between vortices. The mixing within vortices is also enhanced with increasing Taylor number as a result of increased stretching and folding within a vortex. © 1998 Published by Elsevier Science B.V.

*Keywords:* Mixing; Transport; Taylor–Couette flow

## 1. Introduction

Mixing in Taylor–Couette flow is important for catalytic chemical reactors, rotating filtration devices, and bioreactors, all based on an inner cylinder rotating within an outer shell [1]. The idea in many of these devices is to mix the fluid in the annulus while minimizing localized shear stresses. These devices are often operated in the wavy vortex flow regime based on practical experience. Recent measurements of the velocity field in wavy Taylor–Couette flow have shown that, unlike non-wavy vortex flow, wavy vortices are not independent toroidal cells [2]. Instead, for wavy flow in a vertical cylindrical Couette flow device, regions of upward (downward) deformation of a vortex correspond to regions of upward (downward) axial flow. These regions progress around the cylinder at the same speed as the azimuthal travelling wave. Thus in any given radial–axial plane, over the period of one azimuthal wave, there is initially an upward flow winding around the vortices, followed by flow into alternate vortices from adjacent vortices, followed by downward flow winding around the vortices, completing the cycle with flow out of alternate vortices into adjacent vortices (for example see Fig. 1(c). Up to 50% of the volume of a vortex can be transported into and out of a vortex in one azimuthal wave period. In addition to the axial fluid transport, the vortices oscillate both axially, as is evident from flow visualization, and radially.

* Corresponding author.
[1] Present address: ITMS, Univerität Stuttgart, Stuttgart, Germany.
[2] Present address: Department of Chemical Engineering, Rutgers University, Piscataway, NJ, USA.


*PII* S0167-2789(98)00149-3

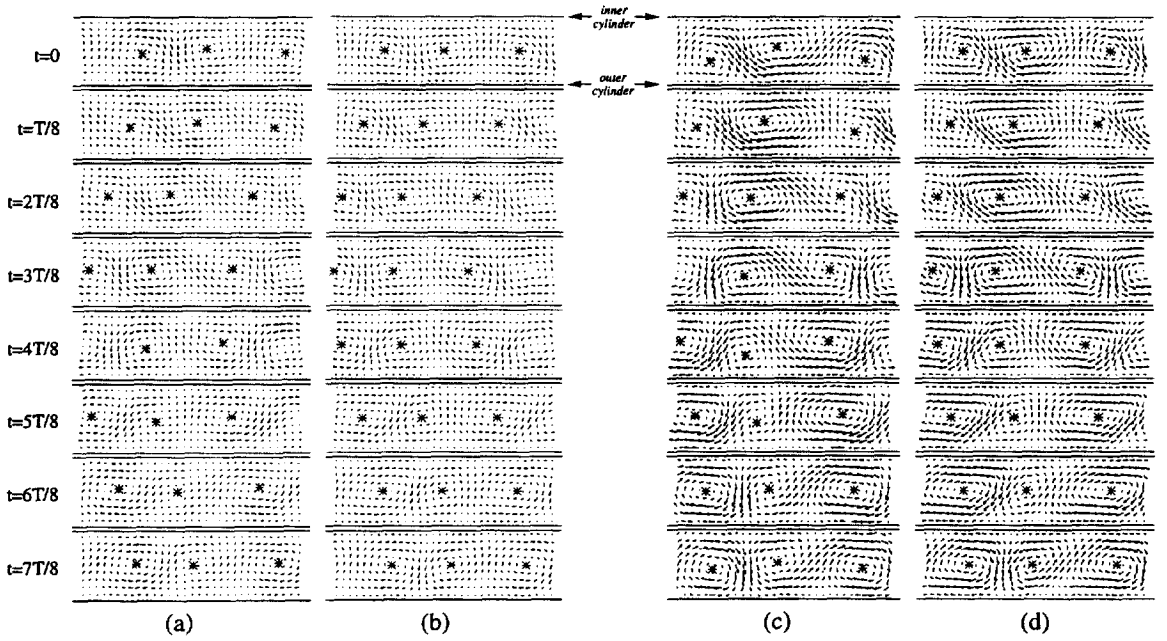


Fig. 1. A comparison between experimentally measured velocities and model results in a radial–axial plane over the period of one azimuthal wave. Time progresses from top to bottom. In each frame the inner rotating cylinder is the upper line, and the outer stationary cylinder is the lower frame (a) experiment, $Ta = 131$; (b) model , $Ta = 131$; (c) experiment, $Ta = 253$; (d) model, $Ta = 253$.

Prior to these recent measurements, several models of particle motion in Taylor–Couette flow and the related Bénard convection flow have been presented. Broomhead and Ryrie [3] and Ryrie [4] considered the transport of fluid particles in a model of Taylor vortex flow near the onset of the wavy instability. By adding small temporally and spatially varying periodic disturbances to an axisymmetric model of non-wavy vortex flow, these authors were able to devise a velocity field with travelling azimuthal waves. Based on this model, they were able to show that transport between vortices is possible even in the absence of molecular diffusion and that particles passing from one vortex to another follow chaotic trajectories, resulting in an enhanced effective diffusivity, or axial dispersion. Solomon and Gollub [5,6] similarly demonstrated enhancement of diffusivity in time-periodic Bénard convection both experimentally and via perturbations of a two-dimensional vortex model. A comparison [7] of their transport properties with experimental results showed good agreement. Ashwin and King [8] used a very different approach in which they tracked fluid particles computationally in the velocity field from the perturbation solution for wavy Taylor vortex flow in a narrow gap just above the onset of waviness [9]. Their results indicated that while some particles wind around adjacent vortices, the cores of adjacent vortices are isolated from one another. Rudman [10] found similar trapping of particles in vortex cores based on tracking fluid particles in numerically modeled wavy vortex flow.

In this paper we use an approach based on modeling the axial and radial velocity components in a radial–axial plane measured using Particle Image Velocimetry (PIV) by Wereley and Lueptow [2]. We first devise a two-dimensional stream-function model of wavy vortex flow (WVF) that matches the experimentally measured vortex distortion and fluid transport between vortices. Then we track fluid particles computationally in this velocity field. This approach differs significantly from the Broomhead and Ryrie [3], Ryrie [4], or Rudman [10] approaches in that the velocity field is based on actual experimental results. Thus, the degree of vortex distortion and transport

between vortices is derived from physical measurements rather than analytically simple perturbations of non-wavy vortices or computational models. Furthermore, our approach permits us to consider flow conditions well above the onset of travelling azimuthal waves. This differs from the studies of Broomhead and Ryrie [3], Ryrie [4], or Ashwin and King [8], which are inherently limited to conditions very near the onset of the azimuthal waviness. Finally, we were able to consider the wide-gap case, whereas Ashwin and King [8] were necessarily limited to infinitesimal gap widths. Our objective here is to investigate the non-turbulent transport and mixing processes in an experimentally motivated model of wavy Taylor vortex flow. The work presented in this paper is an example of matching experimental data with a model, from which further information can be extracted.

In Section 2, we describe the model flow and compare the velocity field that it generates with experimental data. In Section 3, we evaluate the mixing rate and uniformity predicted by the model, after which we evaluate the effective diffusivity, or axial dispersion, in the model flow.

## 2. Stream function model of wavy vortex flow

Available experimental velocity fields include measurements of the axial and radial components of velocity, but not the azimuthal velocity. Consequently, we devise a two-dimensional velocity field to model wavy vortex flow and subsequently track particles. Without the azimuthal velocity component, the experimentally measured radial–axial velocity field cannot be used directly for particle tracking. The utility of a two-dimensional approximation relies on the assumption that mixing and transport are dominated by the radial and axial velocities in wavy vortex flow, with the azimuthal velocity acting principally to distribute the fluid axisymmetrically (on average) around the annulus. A similar assumption was made by Solomon and Gollub [5] for a successful model of transport in time-periodic Bénard convection [7]. Furthermore, our interest is in the axial transport and mixing of the fluid, and experiments in turbulent Taylor–Couette flow indicate that the time scale for transport in the radial and azimuthal directions is short compared to that in the axial direction [11]. While our analysis is for wavy vortex flow, not turbulent flow, the same relationship for the time scales may be expected to occur, supporting the notion that the azimuthal velocity has little effect on the axial transport.

The experimentally measured velocity fields of wavy vortex flow that we model are shown in Figs. 1(a) and (c) for two Taylor numbers with the corresponding model velocity fields shown in Figs. 1(b) and (d), respectively. Each column of figures shows from top to bottom eight realizations of the velocity vectors in a radial–axial plane uniformly distributed over the period of one azimuthal travelling wave. After the lowest frame, the cycle repeats. The upper line in each frame is the wall of the inner rotating cylinder and the lower line is the wall of the outer stationary cylinder. Vortex centers, determined from the interpolated position of the minimum axial and radial velocities, are marked with asterisks.

The WVF cycle can be described most easily with reference to the middle vortex for the experimental results at $Ta = 253$, shown in Fig. 1(c). Although the Taylor number, which relates the centrifugal forces to the viscous forces, has several different forms, we use $Ta = r_i \Omega d/\nu$, where $r_i$ is the radius of the inner cylinder, $\Omega$ is the rotational velocity of the inner cylinder, and $d$ is the gap between the cylinders, and $\nu$ is the kinematic viscosity. This form of the Taylor number, often called a rotating or inner Reynolds number, is used because it is simple and consistent with the form used in several recent studies [12,13]. The cycle begins with fluid from the inner part of the left vortex flowing into the middle vortex and toward the outer cylinder. Simultaneously, fluid from the middle vortex moves into the right vortex and toward the inner cylinder. The result is that fluid winds around the outer side of the middle vortex from left to right. The flow out the right side of the middle vortex ends in the second frame, so that now the middle vortex is gaining fluid from the left vortex without losing any fluid. By the third frame, an inward flow from the right vortex also feeds fluid into the middle vortex. The flow into the middle vortex decreases in the fourth frame

as the flow in from the left vortex ends. In the next four frames the process reverses, beginning with flow around the inner side of the middle vortex from right to left, followed by flow out of the middle vortex to the left, then flow out to the left and right, and finally to the right only. Of course, the middle vortex loses the same amount of fluid during the second half of the cycle that it gains in the first half, and the size of the vortex oscillates correspondingly. The second half of the cycle (frames 5–8) appears identical to the first half of the cycle (frames 1–4) reflected either about an outflow boundary between the left and middle vortices or about an inflow boundary between the middle and right vortices. This is called "shift-and-reflect" symmetry [14].

We begin the development of our model of WVF with a stream function $\Psi(x, y)$ formulated by Chandrasekhar [15] for two-dimensional, counter-rotating rolls bounded by parallel walls, originally devised as a model for Bénard rolls

$$\Psi(x, y) = \frac{A}{k} \sin(kx) W(y), \tag{1}$$

where $x$ and $y$ correspond to the axial and radial coordinates normalized by the gap width $d$, $A$ is an amplitude, $k$ is a wave number non-dimensionalized by the gap $d$ between the parallel plates (at $y = \pm 0.5$), and $W(y)$ is a specific function provided by Chandrasekhar [15] that satisfies the no-slip boundary condition at the walls. $W(y)$ and its derivative vanish at $y = \pm 0.5$.[3]

Eq. (1) results in square vortical cells, but the experimental vortex cells have substantial distortion from a square shape, as shown in Fig 1(c). This distortion is a function of both space and time due to the time periodic nature of the azimuthal waviness. Eq. (1), modified to account for this distortion, results in the following equation:

$$\begin{aligned}\hat{\Psi}(x, y, t) = \frac{A}{k}[1 + j(x, y, t)] \\ \times \{\sin[k(\hat{x} + \delta \sin(k\hat{x}))] - h(t)\} \\ \times W(y),\end{aligned} \tag{2}$$

where

$$\hat{x} = x - g(x, y, t), \tag{3a}$$

$$\begin{aligned}g(x, y, t) = [1 - f(x)]g_{\text{out}}(y, t) + f(x) \\ \times g_{\text{in}}(y, t),\end{aligned} \tag{3b}$$

$$g_{\text{out}}(y, t) = \alpha \sin(\omega t + \tfrac{1}{2}\pi) + \beta y \sin(\omega t + \pi), \tag{3c}$$

$$g_{\text{in}}(y, t) = \alpha \sin(\omega t + \tfrac{1}{2}\pi) + \beta y \sin(\omega t + \tfrac{1}{2}\pi), \tag{3d}$$

$$f(x) = \tfrac{1}{2}[1 - \cos(kx)], \tag{3e}$$

$$h(t) = \eta \sin(\omega t + \tfrac{7}{8}\pi), \tag{4}$$

$$\begin{aligned}j(x, y, t) = \varphi \sin(\omega t + \tfrac{7}{8}\pi) \\ \times \{\sin[k(\hat{x} + \delta \sin(k\hat{x}))] - h(t)\}.\end{aligned} \tag{5}$$

These equations, although collectively abstruse, are individually quite straightforward to understand. Here $\omega$ is the frequency of the travelling wave associated with the azimuthal waviness. The parameters $A$, $k$, $\delta$,$\alpha$,$\beta$,$\eta$, and $\varphi$ are numerical values adjusted to match specific characteristics of the experimental velocity field. The terms $j(x, y, t)$, $\delta$, $g(x, y, t)$, and $h(t)$ distort the vortex field in different ways. The form of Eq. (1) becomes evident in Eq. (2) when these terms approach zero. A brief description of each of the distortions of the vortex represented in Eqs. (2)–(5) follows.

1. *Angled boundaries between vortices and axial displacement of vortices.* The boundaries between vortices in the velocity field for Eq. (1) are at right angles to the bounding walls and are at fixed axial positions. In the experimental velocity fields for WVF shown in Figs. 1(a) and (c) the boundaries are angled with respect to the walls with the angle depending periodically on the time during the period of the azimuthal wave. Furthermore, the angle of inflow boundaries between vortices is not in phase with the angle of outflow boundaries. In addition, the boundaries move axially in a periodic fashion. The function

[3] Presumably due to numerical round-off errors in the original evaluation of the numerical coefficients in $W(y)$, Chandrasekhar's original values for $W(\pm 0.5)$ are slightly different from zero (Eq. (218) of Chap. II in [15]). To compensate for this problem a small constant ($-1.75371244 \times 10^{-4}$) was added to Chandrasekhar's original equation for $W(y)$ to enforce a value of zero for both $W(y)$ and its derivative at the walls. To accommodate this modification, the walls were repositioned at $y = \pm 0.4999537$. Without this correction, marker particles tended to bleed away from the flow boundaries.

$g(x, y, t)$ in Eq. (3a) accounts for the angle and axial motion of the boundaries. The boundary distortion functions $g_{out}(y, t)$ and $g_{in}(y, t)$, Eqs. (3c) and (3d), represent the axial shift and angling of boundaries for outflow and inflow boundaries, respectively. The parameter $\alpha$, which is measured directly from the experimental results, is related to the periodic axial displacement of the vortices, or wave height, which is in phase for outflow and inflow boundaries. The phase of the axial displacement is set for convenience in matching the experimental data. The parameter $\beta$, also measured directly from the experimental results, is related to the periodic angling of the vortex boundaries, which is 90° out of phase for outflow and inflow boundaries. The function $f(x)$, Eq. (3e), multiplying the boundary distortion equations in Eq. (3b) results in the outflow distortion function $g_{out}(y, t)$ having a strong influence at outflow boundaries, or $kx = 2n\pi$, while the inflow distortion function $g_{in}(y, t)$ has a strong influence at inflow boundaries, or $kx = (2n + 1)\pi$ (where $n$ is an integer).

2. *Relative shift of vortex centers.* Experimental [2,16,17] and computational [14,18] studies of both non-wavy and wavy vortex flow show that outflow regions between vortices are stronger than inflow regions. As a result of mass conservation, the centers of vortices on either side of an outflow region must be closer together than the vortices on either side of an inflow region. Since vortex centers are extrema of the stream function, this requires a slight deformation of the position of the extrema while maintaining the periodicity and smoothness of the stream function. One way to achieve this is to use an analytic method proposed by Shinbrot, et al. [19]. In this method, if $p(x)$ is a scalar function that vanishes at two bounds $x_1$ and $x_2$, then

$$\hat{p}(x) = p(x + \delta p(x)) \tag{6}$$

is a one-parameter family of the deformed function lying within the same bounds. Applying Eq. (6) to $p(x) = \sin(kx)$ results in

$$\hat{p}(x) = \sin[k(x + \delta \sin(kx))]. \tag{7}$$

The minima and maxima of this function, which correspond to the positions of the vortex centers on either side of an outflow boundary, are shifted toward one other. Applying this method to the inner square brackets of Eq. (2) results in shifting the vortex centers on either side of an outflow boundary closer together than the vortex centers on either side of an inflow boundary. Judicious choice of the parameter $\delta$ matches the shift of vortex centers of the model to experimental data.

3. *Growth/shrinkage of vortices.* The experimental results indicate that the vortices grow and shrink periodically with the azimuthal waviness. This occurs because at certain times during the cycle, fluid flows out of a vortex into adjacent vortices, while one-half cycle later fluid flows back into the vortex from the same adjacent vortices. As a result, vortices grow and shrink out of phase with respect to their neighbors. The quantity in curly brackets in Eq. (2) defines the axial extent of the vortex cells. For a sine wave the positive portion of the sine represents the axial extent of one cell, while the negative portion of the sine represents the axial extent of the adjacent vortex. Including the quantity $h(t)$ within the brackets shifts the zero-crossing of the sine wave, resulting in one cell has a greater axial extent than its neighbors, without changing the axial wavelength of any vortex pair. Making $h(t)$ dependent on the period of the azimuthal wave, Eq. (4), requires alternate vortices to grow and shrink during each wave period. The degree of growth and shrinkage can be adjusted through the parameter $\eta$ to match the vortex size to experimental data. Note that the phase of vortex cell growth is used to conveniently match the experimental results.

4. *Magnitude correction.* A side effect of the procedure used to control the size dynamics of the vortices is a change in the magnitude of stream function $\hat{\Phi}(x, y, t)$. The function $j(x, y, t)$ is introduced to compensate for this change. Of course, this function must have the same time dependence as $h(t)$, so the argument of the sine in $j(x, y, t)$ (Eq. (5)) is identical to that of $h(t)$ (Eq. (4)). Furthermore, the function $j(x, y, t)$ must vanish at boundaries between vortices. As a result, it is convenient to give $j(x, y, t)$ the same form as the term in curly brackets in the stream function, Eq. (2), to force $\hat{\Psi}$ to vanish at vortex boundaries. The amplitude $\varphi$ is adjusted to match experimental results.

Now there are seven parameters, $A, k, \delta, \alpha, \beta, \eta$, and $\varphi$, that must be matched to experimental velocity data. Superficially, it may appear that with seven parameters the model velocity field could be matched to the experimental velocity field quite arbitrarily. In fact, all of the parameters except $\varphi$ are measured directly from the experimental velocity field and are not subject to interpretation. The vortex strength $A$ is determined by matching the dimensionless quantity $(v_{\text{vortex}}T/d)$ for the model and the experimental data, where $v_{\text{vortex}}$ is the absolute value of the axial velocity component at the axial position corresponding to the vortex center averaged over the gap width, and $T$ is the period of the azimuthal travelling wave. The wave number $k = 2\pi d/\lambda$ is measured directly from experimental wavelength $\lambda$ for a vortex pair. The value for $\delta$ is based on the experimentally measured distance between vortex centers on either side of a vortex boundary averaged at eight times during the period of one azimuthal wave. The wave height is directly measured from the experimental data and is used for the value of $\alpha$. The parameter related to the angle of the boundaries, $\beta$, is less easily derived from the experimental data, since the experimental data is for a three-dimensional flow and the model is inherently two-dimensional. Hence, the model satisfies continuity in two dimensions, while the experimental flow is divergence-free in three dimensions. Consequently, the experimental results can have a net axial flow in the axial–radial plane, which cannot occur in the model. Instead of matching the angle of the boundary, we match the maximum axial velocity at the midpoint of the annular gap and midway between adjacent vortices normalized by $v_{\text{vortex}}$. To do this the parameter $\beta$ is varied until these quantities agree in both model and experiment. This method results in matching the maximum axial velocity, not the maximum axial flow rate, between adjacent vortices. The vortex size parameter $\eta$ is adjusted to directly match experimental minimum and maximum vortex sizes throughout an azimuthal wave period. The only parameter which could not be systematically measured from the experimental data is the compensation factor $\varphi$, which accounts for the change in magnitude of the stream function resulting from controlling the size of the vortices. This parameter was adjusted by trial and error to best match the model to the experimental results.

Table 1
Parameters used in model

| Parameter | $Ta = 131$ | $Ta = 253$ |
|---|---|---|
| Vortex strength ($A$) | 0.2077 | 0.2628 |
| Wavenumber ($k$) | $\pi + 0.097$ | $\pi - 0.1496$ |
| Center position ($\delta$) | 0.06 | 0.08 |
| Wave height ($\alpha$) | 0.4225 | 0.2545 |
| Angling at boundaries ($\beta$) | 0.55 | 0.70 |
| Vortex size ($\eta$) | 0.3 | 0.6 |
| Compensation ($\varphi$) | 0.2 | 0.2 |

The seven parameters were matched at Taylor numbers $Ta = r_i\Omega d/\nu = 131$ and 253. For an experimental radius ratio $r_i/(r_i + d) = 0.83$, the lower Taylor number corresponds to wavy vortex flow just above transition and the higher Taylor number corresponds to the condition for maximal fluid transfer between adjacent vortices for wavy vortex flow [2]. Values for the parameters under these conditions are given in Table 1.

Eq. (2) with Eqs. (3)–(5) is easily differentiated to obtain analytic functions describing the velocity field at any location and time. A comparison of the model velocity field with the experimentally measured velocity field is shown in Fig. 1 for two Taylor numbers. The model captures the essential elements of the velocity field including the winding around vortices, the axial oscillation of the vortex centers, and the flow into and out of any particular vortex with the corresponding change in vortex size. Note, however, that the model velocity field is purely phenomenological. By virtue of its stream function representation, it satisfies continuity. But it does not necessarily satisfy momentum conservation.

Fig. 2 shows the streamlines for $Ta = 131$ and 253 at successive phases of the azimuthal wave (as in Fig. 1). The influence of several of the parameters is evident. For instance, the angle of the boundaries between vortices is steeper for $Ta = 253$ than for $Ta = 131$, as reflected in the different values of $\beta$. The vortices also vary more in size for $Ta = 253$ than for $Ta = 131$, as reflected in the value of $\eta$. But the amplitude of the waviness, most evident in the axial variation in the vortex centers marked by an asterisk,

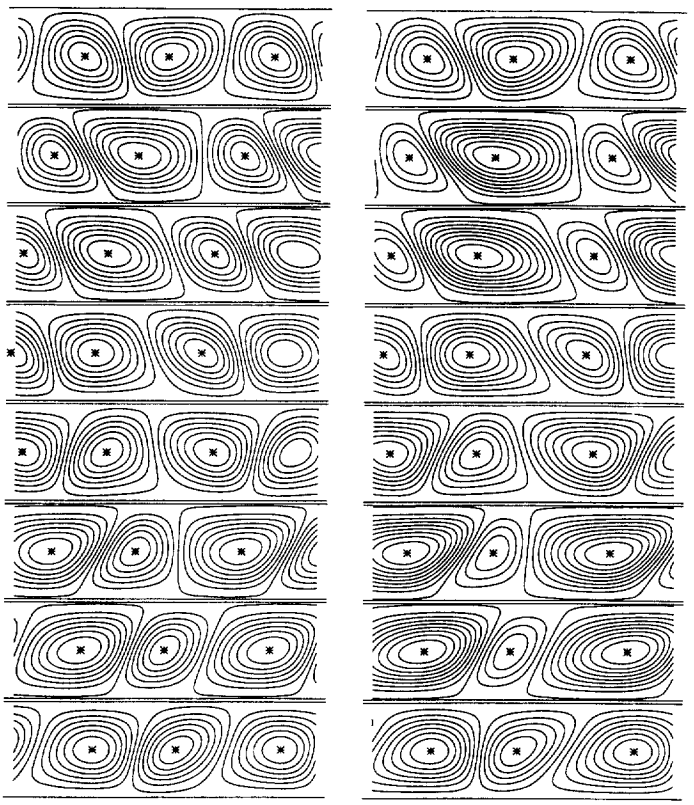


Fig. 2. Streamlines of the model flow in a radial–axial plane over the period of one azimuthal wave. Time progresses from top to bottom. In each frame the inner rotating cylinder is the upper line, and the outer stationary cylinder is the lower line: (a) $Ta = 131$; (b) $Ta = 253$.

is greater for $Ta = 131$ than for $Ta = 253$, as reflected in the parameter $\alpha$. The remaining parameters, $A$, $k$, $\delta$, and $\varphi$, do not differ greatly for the two cases and their influence is less evident in the figure.

## 3. Mixing

From kinematical standpoint, mixing is the stretching and folding of material lines (for two-dimensional flows) or surfaces (for three-dimensional flows). To investigate mixing (and transport) in the flow field we track passive particles.[4] Mixing can be observed by marking particular particles in a region of the flow. This "dyed" region can stretch and fold by advection. Such a numerical experiment is shown in Fig. 3 for $Ta = 253$. Here an initial line of 5000 tracer particles along the mid-line of the annulus at $t = 0.125T$ is allowed to advect for nearly four periods of the azimuthal wave. The axial extent of the region shown in the figure covers two vortices with periodic boundary conditions, so that particles leaving the flow domain on the right re-enter the domain on the left. Folding is evident, most easily observed at $t = 1T$. Further,

[4] Thus, it is necessary to integrate $\mathrm{d}\boldsymbol{x}/\mathrm{d}t = \boldsymbol{u}(\boldsymbol{x})$, where $\boldsymbol{u}(\boldsymbol{x})$ is given by the spatial derivatives of the stream function. A fourth order Runge–Kutta method was used to track particle positions using a time step of $0.0125T$, where $T$ is the period of the azimuthal traveling wave. This time increment generated approximately 100 steps in one orbit around a vortex center at the highest vortex strength modeled.

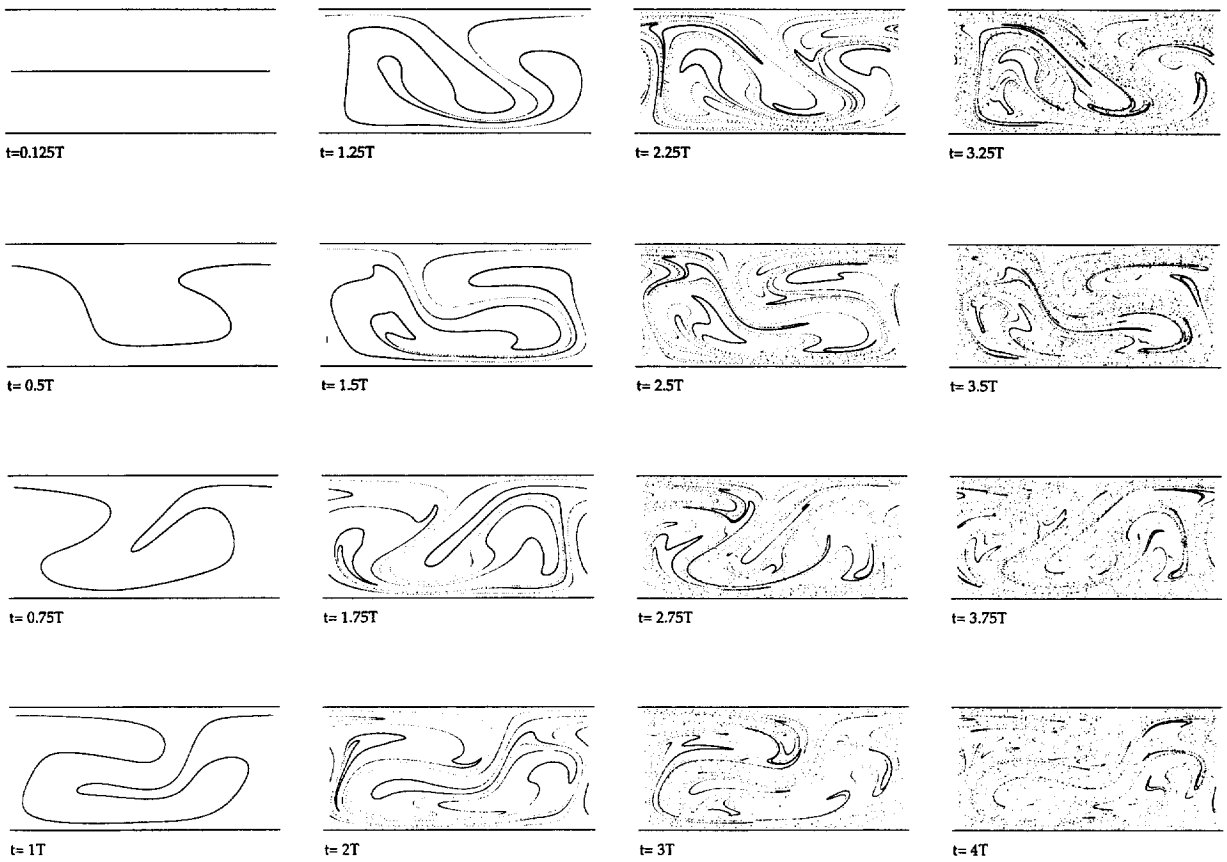


Fig. 3. The time evolution of a line of 5000 particles initially along the midpoint of the annulus at $t = 0.125T$ for $Ta = 253$.

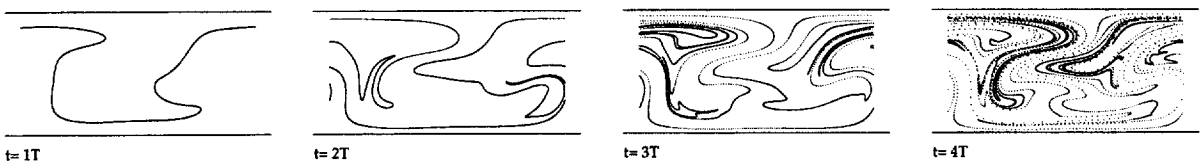


Fig. 4. The time evolution of a line of 5000 particles initially along the midpoint of the annulus for $Ta = 131$

note the self-similar structure exhibited by folded elements as time evolves in steps of $T$. For example, the relatively thin tongue enclosed by a large fold of a horizontal horseshoe shape at $t = 1T$ appears again at $t = 2T$, $3T$ and $4T$ at successively smaller scales. A goal of mixing is the reduction of length scales, which can be efficiently accomplished by this stretching and folding. The flow in Fig. 3 has particularly good mixing characteristics as evidenced by the high fraction of the area that is penetrated by marker particles and the uniform dispersion of particles. The existence of horseshoe structures [20] indicates effective stretching and folding and implies chaotic mixing. For comparison, similar results for $Ta = 131$ are shown in Fig. 4 for fewer time instants. The mixing is not as rapid at the lower Taylor number, although horseshoes and successively refined striations are again seen in this figure.

The stretching can be quantified in terms of the finite time Lyapunov number, calculated numerically

Table 2
Lyapunov numbers

| $Ta$ | $\Lambda_N$ at $N = 1600$ |
|---|---|
| 131 | 2.8 |
| 192 | 3.5 |
| 253 | 4.4 |

using the procedure of Wolf et al. [21]. Lyapunov numbers for tracer particles initially placed at the middle of the annulus at three different Taylor numbers are displayed in Table 2. The Lyapunov number typically varies with the number of wave periods used in the calculation, up to about 200 wave periods. Calculations of the Lyapunov number for 200–1600 wave periods produced essentially a constant value for a given Taylor number. The calculations for $Ta = 192$, which is midway between the Taylor numbers for which model parameter were calculated as indicated in Table 1, were based on linear interpolation of the parameters in Table 1. The Lyapunov numbers are unambiguously greater than unity, supporting the conclusion that the trajectories in the model are chaotic. The magnitude of the Lyapunov number provides a measure of how fast interfacial lines between constituents in the mixing process are produced, so the higher Taylor number should provide more rapid mixing, consistent with the qualitative results shown in Figs. 3 and 4.

Further insight into the time-periodic model of WVF can be gained from a stroboscopic surface of section, obtained by plotting $(x(t), y(t))$ for a particle at $t = t_0 + nT$, where $n$ is an integer. A typical stroboscopic section is shown in Fig. 5(a) for $Ta = 131$. During 100 successive cycles, 1000 particles initially placed midway between the upper and lower simulation boundaries become stochastically dispersed throughout the available area. For this Taylor number, there are evidently no regular regions of any significant size, and mixing appears to be uniform as well as rapid. Systematic tests throughout the range of Taylor numbers $131 \leq Ta \leq 253$ at intervals of $\Delta Ta \cong 6$, indicate only one set of Taylor numbers which generate regular regions of non-trivial size. In a range of Taylor numbers $155 \leq Ta \leq 204$, elliptic islands are found as shown in Fig. 5(b). Even these islands are rather small, making up only a few percent of the flow field.

## 4. Axial dispersion

In the structurally related case of time-periodic Bénard flow, Solomon and Gollub [5,6] reported experimental observations suggesting that transport between rolls can be modeled as a diffusion process. To differentiate this process from molecular diffusion, we refer to this transport as dispersion. Solomon and Gollub obtained a dispersion coefficient 1–3 orders of magnitude larger than would be expected from molecular diffusion alone. Furthermore, a numerical investigation of a model of WVF at the onset of instability by Broomhead and Ryrie [3] suggests a dispersion transport process. Insight into the axial transport in WVF can be obtained by tracking particles over time. Fig. 6 shows the positions of 20 000 particles initially distributed along a single radial line in the outflow region between a vortex pair after five azimuthal wave periods. The small sparse region at the inner cylinder wall (upper line) approximately marks the axial position of an outflow boundary, and the sparse region at the outer cylinder wall (lower line) approximately marks the position of an inflow boundary. Using this as a guide, it is evident that at $Ta = 131$, particles have penetrated six vortices in five wave periods, whereas at $Ta = 253$, particles have penetrated eight vortices. At the same time, a larger fraction of the area is filled with marker particles at $Ta = 253$ than at the lower Taylor number, indicating better mixing within vortices as well as more efficient axial transport between vortices. By contrast, at low Taylor number the dispersion within a vortex can be described as a non-uniform distribution of segregated filaments with "tongues" extending into adjacent vortices.

The axial transport can be quantitatively compared by calculating of histograms of particles numbers along the length of the annulus, shown in Fig. 7 at $t = 15T$. Here the axial coordinate is normalized by the annular gap width so that a vortex pair spans a region of approximately $\Delta x = 2$. At the higher Taylor number, sharp gradients in particle distribution occur at boundaries between vortex pairs ($x = \pm 1, \pm 3$, etc.), while the particle distribution within a vortex pair is relatively uniform ( for $-1 \leq x \leq 1$, $1 \leq x \leq 3$, etc.). By contrast, at the lower Taylor number, boundaries

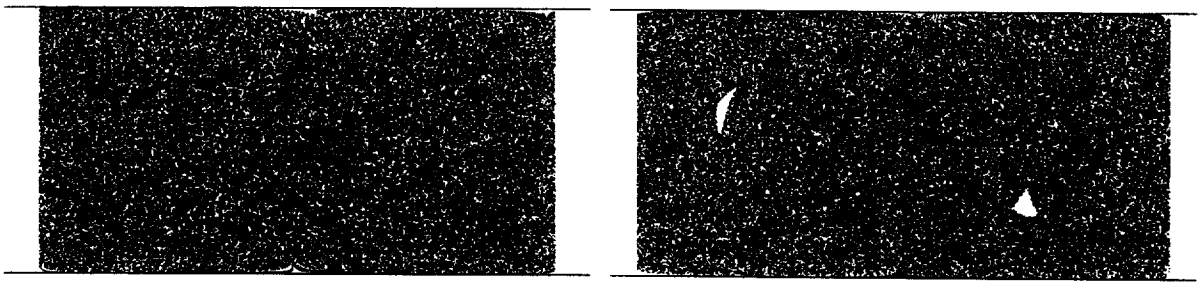

(a) (b)

Fig. 5. Stroboscopic section spanning a pair of vortices; 1000 initial points placed on the line $y = 0$ (midway between the inner and outer cylinder walls) are recorded after each of 100 successive cycles: (a) $Ta = 131$; (b) $Ta = 180$.

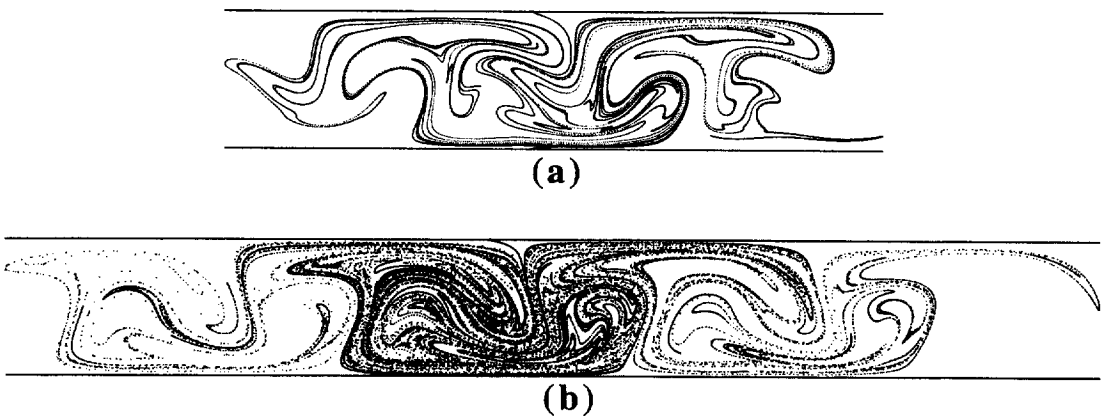


Fig. 6. A snapshot at $t = 5T$ of the positions of 20 000 particles initially distributed along a single radial line in an outflow region: (a) $Ta = 131$; (b) $Ta = 253$.

between vortex pairs are not as clearly defined, and the distribution of particles across a vortex pair is not at all uniform. In longer simulations, we have found that as the simulation time increases to $t = 195T$, the histograms approach a Gaussian character, although the variance grows with Taylor number.

The axial transport can be quantified in terms of an axial dispersion coefficient, also known as an "effective diffusion" coefficient. The coefficient we use is based on the expression given by Broomhead and Ryrie [3],

$$D^* = \lim_{n\to\infty} \left\{ \frac{1}{N} \sum_{j=1}^{N} [x_j(n) - x_j(0)]^2 / 2n \right\}, \qquad (8)$$

where $N$ is the total number of particles and $x_j(n)$ is the axial position of the $j$-th particle at time step $n$. For short times, the axial dispersion coefficient is dependent on the initial placement of particles and the time of release during the period of the azimuthal wave. Two different initial particle distributions were used. In the first case, 2500 particles were placed in the flow distributed along a radial line at each of eight equally spaced times ($t = 0.125T,\ 0.25T, \ldots, 1.0T$) during one azimuthal wave period. Multiple initial particle placements were used to minimize the dependence on the initial release time. In the second case, 20 000 particles were randomly distributed in a single vortex pair at $t = 0.5T$. Although for short times the dispersion coefficient varied significantly between the two methods for small times, by $t = 30T$ both methods resulted in similar values of $D^*$, and by $t = 195T$ the values for the two methods agreed within 2%.

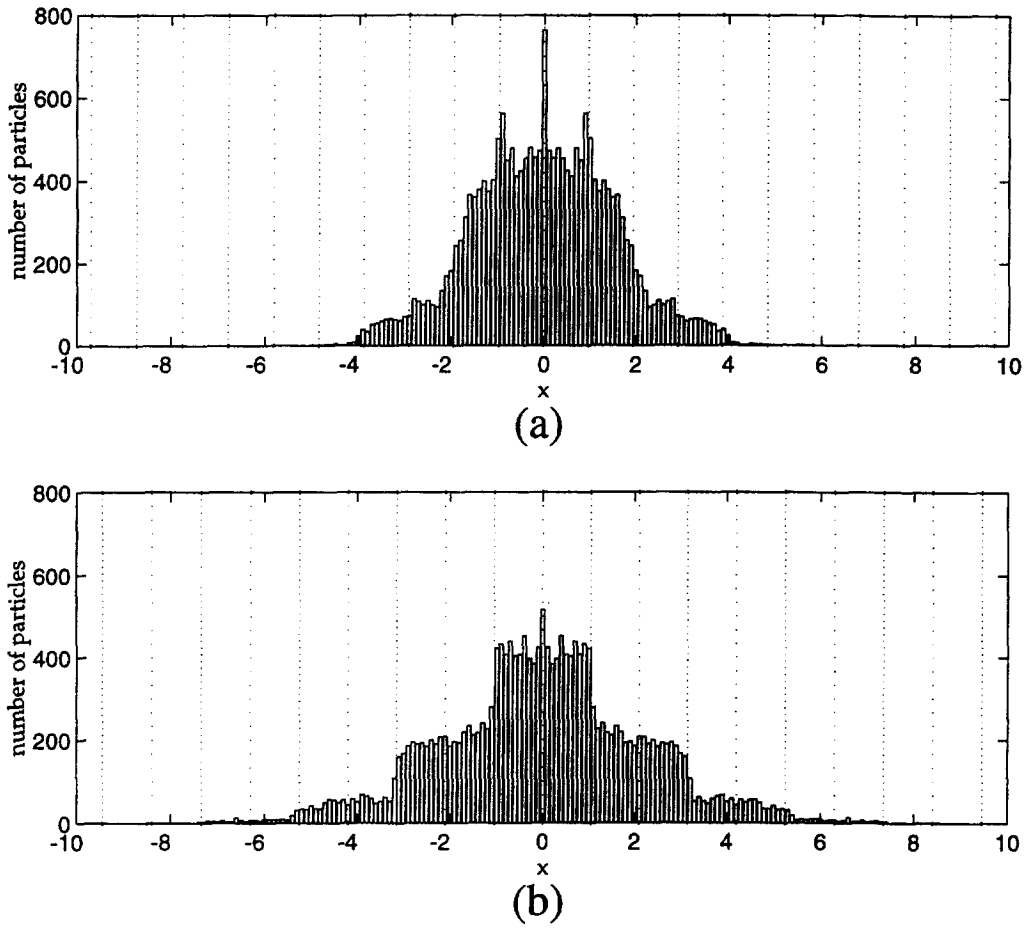


Fig. 7. Histogram of the axial distribution of 20 000 particles at $t = 15T$: (a) $Ta = 131$; (b) $Ta = 253$.

The axial dispersion coefficient at $t = 195T$ averaged for the two methods is given in Table 3. Clearly the axial dispersion due to the WVF is substantially greater at $Ta = 253$ than at lower Taylor numbers. The dispersion coefficients are similar to those found by Rudman [10] for a computational model of wavy vortex flow. Broomhead and Ryrie [3] also found similar dispersion coefficients for a less physical model of WVF over a particular range of the parameter space that they considered. However, in the parameter range where our dispersion coefficients agree with Ryrie [4], we found that nearly the entire flow field was chaotic (based on stroboscopic sections such as those shown in Fig. 5), while she found that less than half of the flow field is chaotic. The difference may be due to the simplicity of the Ryrie model compared to our model.

Table 3

| $Ta$ | $D^*$ | $D(\mathrm{cm}^2/\mathrm{s})$ |
|---|---|---|
| 131 | 0.0075 | 0.0008 |
| 192 | 0.0124 | 0.0026 |
| 253 | 0.0187 | 0.0061 |

The dimensional axial dispersion coefficients, $D$, are also included in Table 3 for comparison to experimental results. These values were based on the parameters in the original flow upon which the model presented here is based [2]. The dimensional values compare well with the extrapolation of measurements of tracer dispersion at low Taylor numbers, which

probably correspond to WVF, although the authors are not clear on this point (Fig. 1 of [1]). Measurements of the dispersion coefficient have also been made at much higher Taylor numbers in the turbulent Taylor vortex flow regime [1,11,22]. In these cases, the axial dispersion coefficient is up to 3 orders of magnitude greater than that for WVF. The mechanism for enhanced transport in turbulent Taylor vortex flow is doubtless intrinsic to the turbulence, whereas the mechanism in wavy vortex flow is axial transport of fluid between vortices.

## 5. Summary

As experimental techniques being applied to classic fluid dynamics problems become increasingly sophisticated, so too should analytic techniques adapt and develop. Our simulation, while neglecting the azimuthal component of velocity, is intended to provide a reasonably accurate model of the mixing and axial transport properties of WVF at higher Taylor numbers and larger gap widths than previous models. Based on the Lyapunov numbers and stroboscopic sections of WVF for $131 \leq Ta \leq 253$, particle paths appear to be chaotic throughout essentially all of the fluid volume. Thus, the fluid mixes efficiently within an individual vortex and this mixing is enhanced as the Taylor number is increased. The rate of axial scalar transport is increased substantially compared to that due to molecular diffusion. The enhancement of transport is largely due to the transfer of well-mixed fluid between adjacent vortices. Increasing the Taylor number above 253 may not result in either faster mixing or more complete transport in the wavy vortex flow regime, because experiments indicate that the maximum transfer of fluid between vortices occurs at $Ta = 253$, with decreasing transfer at both lower and higher Taylor numbers.

## Acknowledgements

This work was partially supported by the National Science Foundation and by the Deutscher Akademischer Austauschdienst (DAAD).

## References

[1] C.M.V. Moore, C.L. Cooney, Axial dispersion in Taylor–Couette flow, AIChE J. 41 (1995) 723–727.
[2] S.T. Wereley, R.M. Lueptow, Spatio-temporal character of non-wavy and wavy Taylor–Couette flow, J. Fluid Mech. 364 (1998) 59–80.
[3] D.S. Broomhead, S.C. Ryrie, Particle paths in wavy vortices, Nonlinearity 1 (1988) 409–434.
[4] S.C. Ryrie, Mixing by chaotic advection in a class of spatially periodic flows, J. Fluid Mech. 236 (1992) 1–26.
[5] T.H. Solomon, J.P. Gollub, Chaotic particle transport in time-dependent Rayleigh–Benard convection, Phys. Rev. A 38 (1988) 6280–6286.
[6] T.H. Solomon, J.P. Gollub, Passive transport in steady Rayleigh-Bénard convection, Phys. Fluids 31 (1988) 1372–1379.
[7] S. Wiggins, Chaotic Transport in Dynamical Systems, Springer, Berlin, 1992.
[8] P. Ashwin, G.P. King, A study of particle paths in non-axisymmetric Taylor–Couette flows, J. Fluid Mech. 338 (1997) 341–362.
[9] A. Davey, R.C. DiPrima, J.T. Stuart, On the instability of Taylor vortices, J. Fluid Mech. 31 (1968) 17–52.
[10] M. Rudman, Mixing and particle dispersion in the wavy vortex regime of Taylor–Couette flow, Preprint, 1997.
[11] W.Y. Tam, H.L. Swinney, Mass transport in turbulent Couette–Taylor flow, Phys. Rev. A 36 (1987) 1374–1381.
[12] P.R. Fenstermacher, H.L. Swinney, J.P. Gollub, Dynamical instabilities and the transition to chaotic Taylor vortex flow, J. Fluid Mech. 94 (1979) 103–128.
[13] C.D. Andereck, S.S. Liu, H.L. Swinney, Flow regimes in a circular Couette system with independently rotating cylinders, J. Fluid Mech. 164 (1986) 155–183.
[14] P.S. Marcus, Simulation of Taylor-Couette flow. Part 2. Numerical results for wavy-vortex flow with one travelling wave, J. Fluid Mech. 146 (1984) 65–113.
[15] S. Chandrasekhar, Hydrodynamic and Hydromagnetic Stability, Oxford University Press, Oxford, 1961.
[16] H.A. Snyder, R.B. Lambert, Harmonic generation in Taylor vortices between rotating cylinders, J. Fluid Mech. 26 (1966) 545–562.
[17] S.T. Wereley, R.M. Lueptow, Azimuthal velocity in supercritical circular Couette flow, Exp. Fluids 18 (1994) 1–9.
[18] H. Fasel, O. Booz, Numerical investigation of supercritical Taylor-vortex flow for a wide gap, J. Fluid Mech. 138 (1984) 21–52.
[19] T. Shinbrot, L. Bresler, J.M. Ottino, Control of transport in a chaotic lattice, Physica D 93 (1996) 191–209.
[20] S. Smale, Differentiable dynamical systems, Bull. Am. Math. Soc. 73 (1967) 747–817.
[21] A. Wolf, J.B. Swift, H.L. Swinney, J.A. Vastano, Determining Lyapunov exponents from a time series, Physica D 16 (1985) 285–317.
[22] Y. Enokida, K. Nakata, A. Suzuki, Axial turbulent diffusion in fluid between rotating coaxial cylinders, AIChE J. 35 (1989) 1211–1214.